Hindawi
Wireless Communications and Mobile Computing
Volume 2019, Article ID 5125287, 7 pages
https://doi.org/10.1155/2019/5125287

Research Article

Planar Lens Antenna for High Data Rate Applications

Daniel Santillán-Haro,[1,2] Daniel Sánchez-Escuderos,[1] Eva Antonino-Daviu,[1] and Miguel Ferrando-Bataller[1]

[1]*Instituto de Telecomunicaciones y Aplicaciones Multimedia (ITEAM), Universitat Politècnica de València (UPV), c/ Cami de Vera, s/n, 46022 Valencia, Spain*
[2]*Facultad de Ingeniería, Universidad Nacional de Chimborazo (UNACH), Avda. Antonio Jose de Sucre km 1.5, Vía a Guano, Riobamba, Ecuador*

Correspondence should be addressed to Eva Antonino-Daviu; evanda@upvnet.upv.es

Received 25 October 2018; Accepted 18 December 2018; Published 4 February 2019

Academic Editor: Daniele Pinchera

A low-profile lens antenna formed by 2 metallic rings with strips short-circuiting both rings is presented. The theory of characteristic modes is used to facilitate the design, optimization, and analysis of the structure. Simulations and measurements are presented for the optimized single-layer metallic lens antenna. Measured results show a large operating bandwidth (14.7% relative -14 dB impedance bandwidth) with a maximum directivity above 13.70 dBi and a return loss better than 14 dB.

1. Introduction

The increase of small cell base stations, wireless access points, laptops, tablets, and smartphones, each with a computing capacity comparable to that of a computer server a decade ago, and the growing demand for multimedia services are leading to an increase in the traffic of associated broadband connections, with high access speed and low latency [1]. From the perspective of the system, these needs require the use of low-profile directive antennas that maximize the gain, and exhibit energy-focusing capability.

Over the past few years, metal lenses have attracted an increasing interest as high-gain antennas in multiple applications. Several types of lenses have been proposed to improve the gain and efficiency of simple radiators. These lenses are commonly designed using periodic structures, such as EBG (Electromagnetic Band Gap) or FSS (Frequency Selective Surfaces). In [2], a nonuniform three-layer FSS lens is presented, whereas, in [3], a metallic luneburg lens is proposed with pin-loaded holes with glide symmetry to increase the equivalent refractive index of the structure.

Periodic structures have also been used to design transmitarrays [4, 5], and reflectarrays [6], based on the analysis of the unit cell with infinitely periodic boundary conditions. In [7, 8], thin planar lenses are proposed for massive MIMO applications, and, in [9], gradient metasurfaces are used to construct a planar lens antenna system. In all cases, the truncation to a finite number of cells from the theoretical infinite number leads to inaccurate results, thereby demanding a costly optimization process.

Alternatively, the design might be carried out using the Theory of Characteristic Modes (TCM). The TCM facilitates the design process because it provides a very clear understanding of the radiation behavior of metal and dielectric bodies [10]. This theory was initially formulated by Garbacz [11] and improved by Harrington and Mautz in [12], where they explained how to compute the characteristics eigenvalues and eigencurrents for a conducting body.

For more than a decade, the TCM has been used to design mobile antennas [13], analyze slotted planar structures [14, 15], study some canonical structures such as spheres or cylinders [16], design wideband omnidirectional antennas [17], or provide design guidelines for open slot antennas embedded in finite platforms [18]. The TCM has also been used to analyze metallic lenses, such as a lens formed by twelve metallic rings distributed in a single-layer in [19], a low-profile lens made of metallic cylinders [20], or a metallic

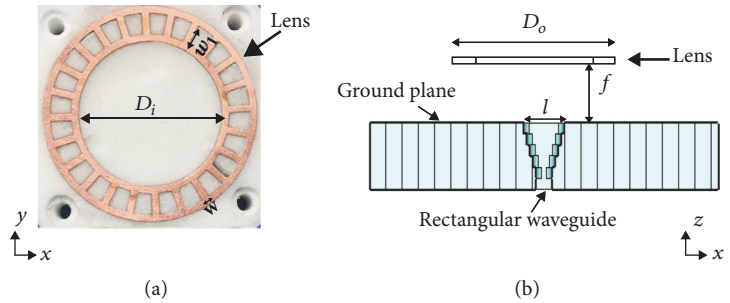

Figure 1: Geometry of the proposed antenna: (a) metallic lens antenna; (b) lateral view.

lens designed with a central circular metallic ring surrounded by a set of eight metallic rings.

In this paper, we propose the use of the TCM not only to analyze but also to design the lens antenna. In particular, the TCM is used to design a single-layer metallic lens antenna formed by two short-circuited metallic rings and fed by a rectangular waveguide. A similar structure was developed in [21], where the results of the simulation of the lens were presented, but in this work we demonstrate the usefulness of the TCM for the design of the lens, presenting measured results as well. Characteristic modes (CM) have been calculated using FEKO [22], and the design of the lens has been performed with CST Microwave Studio [23].

2. Analysis of Characteristic Modes of the Proposed Metallic Structure

2.1. Structure. Considering that the CM analysis is based on the structure without feeder, for the initial dimensions, the lens is modeled as a PEC object identical to that shown in Figure 1(a), with a thickness of 0.35 mm, a width of $w = 1.37$ mm, an inner diameter $D_i = 29.32$ mm ($2\lambda_0$), a shorting strip $w_1 = 4.04$ mm, and an external diameter $D_o = 42.89$ mm ($3\lambda_0$), where λ_0 is the free-space wavelength at the central operating frequency (20.50 GHz). The lens antenna consists of two short-circuited metallic rings, whose sectors are no larger than λ at the design frequency, distributed in twenty-four sectors as shown in Figure 1(a), intended to operate in the 19–22 GHz band. The lens is placed at a distance f from the feeder.

2.2. Analysis of Characteristic Modes. As discussed in [10–12], the TCM provides a physical interpretation of the radiation by a given structure, which is of great help in antenna design. The CM are real current modes ($\mathbf{J}_n$) that are extracted at each frequency from the generalized impedance matrix of the antenna. These modes form a set of orthogonal functions that can be used to expand the total current in the surface of the structure, as described in the following equations:

$$\mathbf{J} = \sum_n \frac{V_n^i \mathbf{J}_n}{1 + j\lambda_n} \tag{1}$$

$$V_n^i = \oint_s \mathbf{J}_n \bullet \mathbf{E}^i ds, \tag{2}$$

where $\mathbf{J}_n$ are the characteristic currents on the conducting body, λ_n are the eigenvalues, and V_n^i is the modal excitation coefficient. Despite $\mathbf{J}_n$ and λ_n being the only two quantities solved in the base equation, there are other physical interpretations of the eigenvalue, such as the characteristic angle (α_n) and the modal significance (MS_n). The characteristic angle (α_n) is associated with each eigenvalue as

$$\alpha_n = 180^\circ - \arctan(\lambda_n). \tag{3}$$

The characteristic angle (α_n) indicates how the phase of a single current changes over the frequency, and can be used to design antennas with a specific phase distribution [10]. The modal significance (MS_n) is an intrinsic property of each mode and is independent of any specific external source. The MS_n provides a convenient way to measure the bandwidth of each characteristic mode, mathematically expressed as

$$MS_n = \left| \frac{1}{1 + j\lambda_n} \right|. \tag{4}$$

The mode is at resonance when the characteristic angle is 180° (α_n=180°) or the modal significance is one (MS_n=1).

The half-power radiating bandwidth of a mode (BW_n) constitutes an important figure of merit to determine the radiation performance of characteristic modes [10]. It can be expressed as $BW_n = (f_U - f_L)/f_{res}$, where f_{res} is the resonance frequency of the mode and f_L and f_U are the lower and upper frequencies, respectively, for a MS_n threshold of $1/\sqrt{2}$. Furthermore, a modal quality factor can be defined from the fractional bandwidth as $Q_{rad,n} = 1/BW_n$ [10].

The modal currents of the first four modes of the proposed metallic structure are illustrated in Figure 2. Black lines have been added to indicate the direction of the currents.

Figure 2(a) shows a very intense current distribution in the short-circuiting strips between the inner and outer rings for Mode 1. The orthogonal modal current (Mode 1') is included in Figure 2(b). Mode 2 presents a vertical current distribution in the two metal rings (see Figure 2(c)), and Mode 3 (see Figure 2(d)) presents a loop inside and outside the total structure. Each modal current maintains this current distribution in the metallic structure over the whole frequency range (19–22 GHz).

The radiated far field of the first four modes is shown in Figure 3. From these radiation patterns it is clear that Mode 1, Mode 1', and Mode 2 are the desirable modes in order

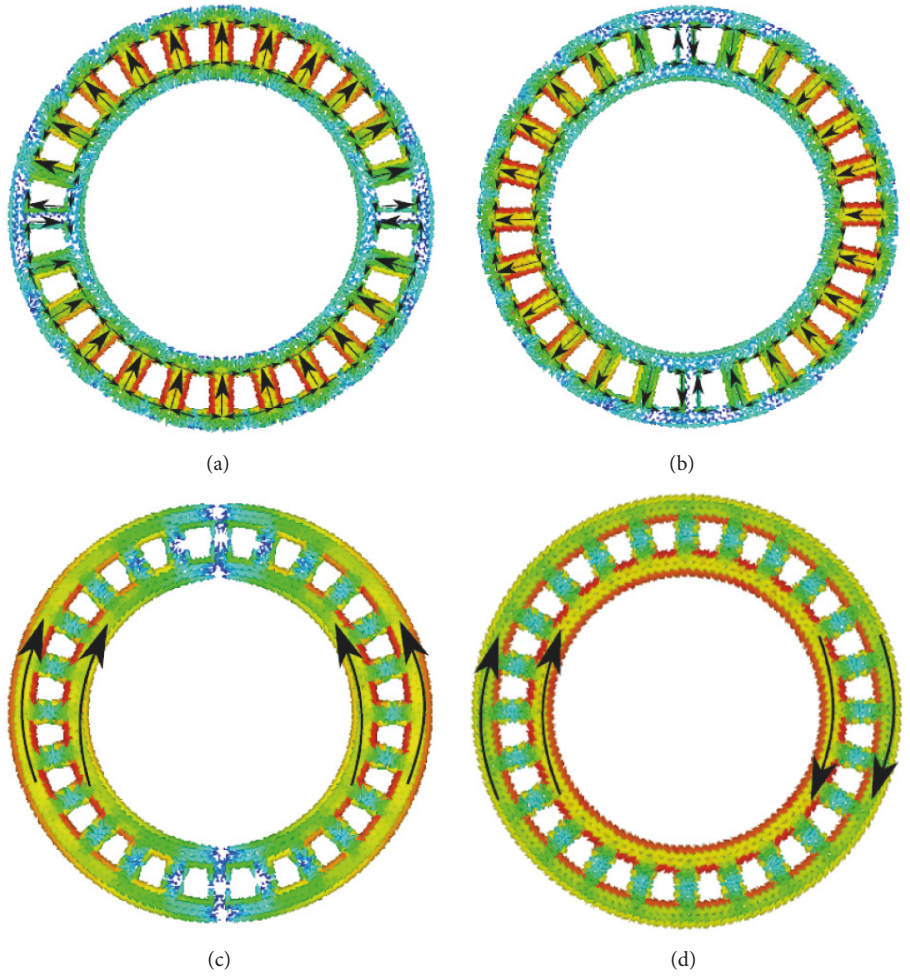

Figure 2: Modal currents of the lens proposed at 20.5 GHz: (a) Mode 1; (b) Mode 1'; (c) Mode 2; (d) Mode 3.

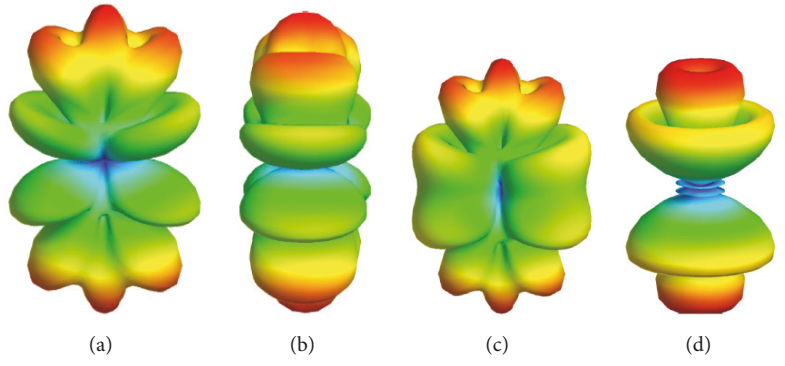

Figure 3: Modal radiation pattern of the proposed lens at 20.5 GHz: (a) Mode 1; (b) Mode 1'; (c) Mode 2; (d) Mode 3.

to obtain a maximum radiation in the broadside direction. However, if a vertically polarized plane wave incides in the lens, only Mode 1 and Mode 2 will be excited.

2.3. Design of the Lens Antenna. As seen, fundamental Mode 1 presents a broadside radiation pattern at the central frequency. In order to excite this fundamental Mode 1, a parametric study of α_n and MS for different lens sizes is performed. The aim is to have a resonance for Mode 1 at the central frequency, together with a large bandwidth.

As a starting point for the design, the structure considered is the one presented in Section 2.1. The two variables of the design are D_i and w_1. The number of sectors in the structure is left fixed, in order to keep the symmetry. Note that,

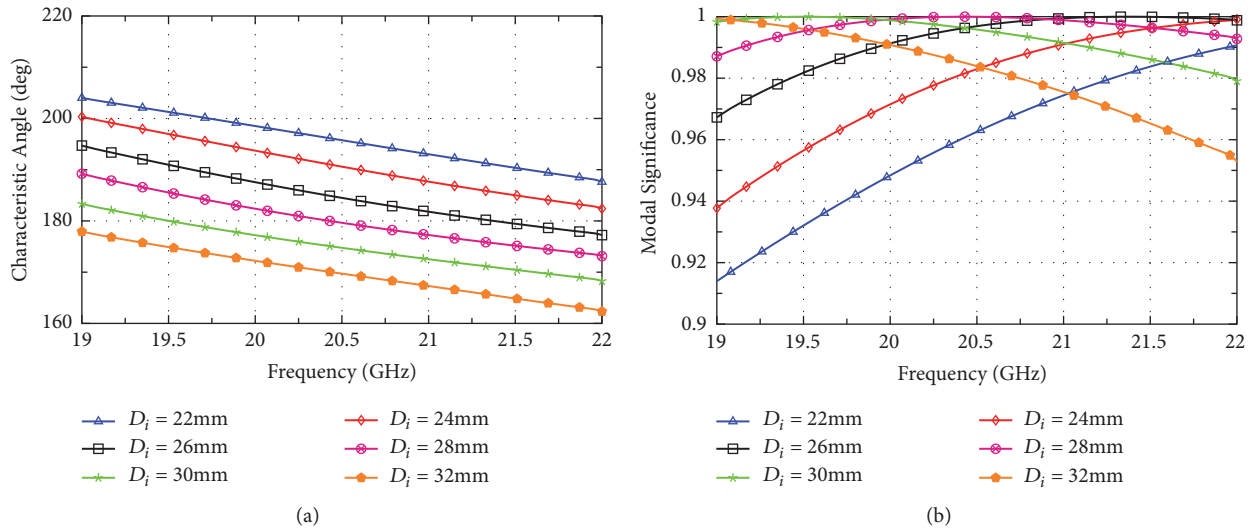

FIGURE 4: Modal parameters of the proposed lens by varying the internal diameter D_i with w_1 = 4.04 mm: (a) characteristic angle Mode 1; (b) modal significance Mode1.

considering w_1 = 4.04 mm and a variable internal diameter D_i, the value of the external diameter of the structure can be found by the relationship $D_o = w_1 + D_i$. With this in mind, we first present the results for a fixed w_1 value (w_1 = 4.04 mm) and D_i ranging between 22 and 32 mm.

Figure 4(a) plots the phase values of Mode 1 for different D_i values. As seen in the band of interest (19–22 GHz), D_i values for the resonance of the structure (α_n=180°) are within the range 26–30 mm. For $D_i \leq 24$ mm, the structure has a capacitive behavior, and for $D_i \geq 32$ mm it has an inductive behavior (α_n <180°).

Figure 4(b) shows the values of modal significance for Mode 1. As can be observed, for D_i = 28 mm, we have values higher than 0.98 in the whole band, which is a very good value above the commonly adopted 0.7 threshold to guarantee a large bandwidth.

From the above results, it can be easily deduced that for D_i = 28 mm there is a resonance at the central frequency 20.5 GHz and a high modal significance for Mode 1.

Figure 5 presents the characteristic angle α_n of the proposed metallic structure by varying D_i and w_1 for Mode 1, at 20.5 GHz. As can be seen, Mode 1 resonates for D_i = 27.87 mm with w_1 = 4.04 mm. There exists other possible values, but these lead to the smallest lens.

Figure 6 represents the contribution of each mode to the total radiated power for the proposed lens with D_i = 27.87 mm and w_1 = 4.04 mm, when excited with a vertically polarized plane wave with normal incidence. As can be seen, at the central frequency, a 60% of Mode 1 and a 40% of Mode 2 generate the total radiated power. Since these two modes have a maximum at broadside direction, the total power field will also have a maximum at this direction.

3. Lens Design

Considering the results obtained in previous section, the optimum values for the metallic lens in order to resonate at

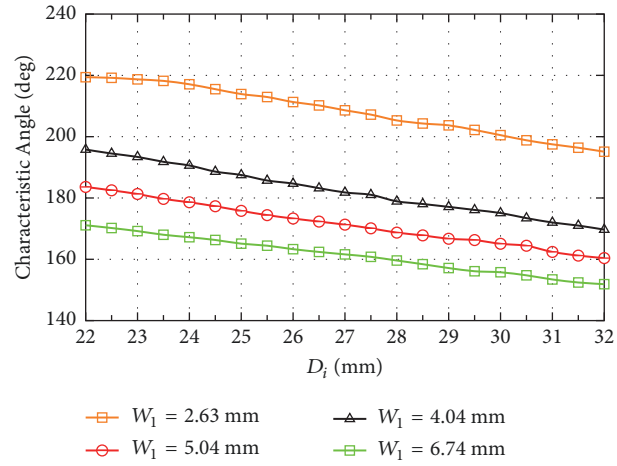

FIGURE 5: Characteristic angle of the proposed lens by varying D_i and w_1 at 20.5 GHz for Mode 1.

20.5 GHz are D_i = 27.87 mm and w_1 = 4.04 mm, which means that the external diameter D_o is 41.43 mm. Note that the width and thickness are the same as in the structure presented in Section 2.1.

The next step is to find the optimal feeding point of the lens. This point corresponds to the distance between the lens and the feeding aperture, where the resulting radiated electromagnetic waves have a plane wave front at the upper level of the metallic structure.

3.1. Plane Wave Analysis (Focal Point). The focal point can be determined using several methods such as geometrical optics used in the Fresnel zone plate [24], or the plane wave incidence described in [19], where a plane wave impinges on the metallic structure. In this work, we use the second method, considering an incident field produced by a plane

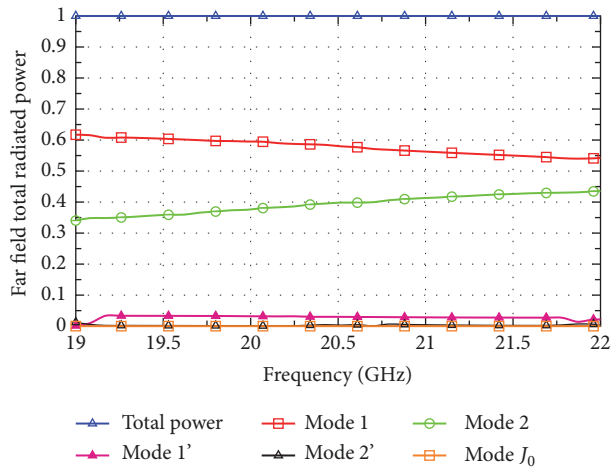

FIGURE 6: Contribution of the each mode to the total radiated power for the proposed lens with $D_i = 27.87$ mm and $w_1 = 4.04$ mm considering plane wave with normal incidence.

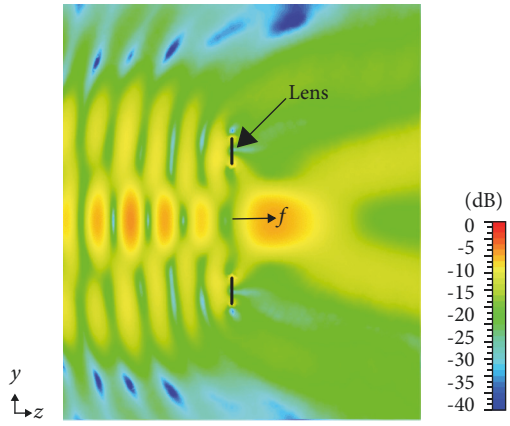

FIGURE 7: Simulation of the plane wave at 20.5 GHz in the proposed lens.

wave propagating in the z direction, the lens being located in the x–y plane. Figure 7 shows the electric field with this configuration at 20.5 GHz. It can be seen that the field is focused on the other side of the metallic structure, at $f = 9.54$ mm from the lens. This is the focus of the lens and is where the feeder must be placed.

The feeder is a square aperture (10.66 mm × 10.66 mm). This size guarantees a −10 dB taper on the edge of the lens. The aperture is placed on a ground plane (90 mm × 90 mm) which only introduces a small ripple in the radiation pattern of the lens. The aperture is fed by a transition of length $l = 10.66$ mm to allow the feeding of the structure by means of a standard rectangular waveguide (WR-42). Figure 8 shows a picture of the prototype. The feeder has been fabricated in aluminum (see Figure 8(a)), while the single-layer lens antenna has been fabricated in a copper sheet, as shown in Figure 8(b), and attached to a foam layer with the same height as the focal distance f (see Figure 8(c)), to guarantee the correct separation between the lens and the feeder.

4. Experimental Results of the Single-Layer Lens Antenna

To validate the performance of the proposed single-layer lens antenna, the S_{11} parameter has been measured. Figure 9 compares measured and simulated results. As can be observed, both results are quite similar, with a good matching ($S_{11} < -14$ dB) from 19 to 22 GHz.

The measured and simulated copolar and crosspolar components of the radiated field are shown in Figure 10. A good measured crosspolar level (below -27 dB) is observed within the main beam of the pattern. The differences between the measured and simulated patterns are caused by an inaccurate characterization of the foam material between the lens and the feeder and, also, by unexpected manufacturing errors.

Figure 11 shows that the maximum measured gain is 14 dBi at 19 GHz, which corresponds to an increase in directivity of 5.23 dB with respect to the measurement of an open-ended square waveguide.

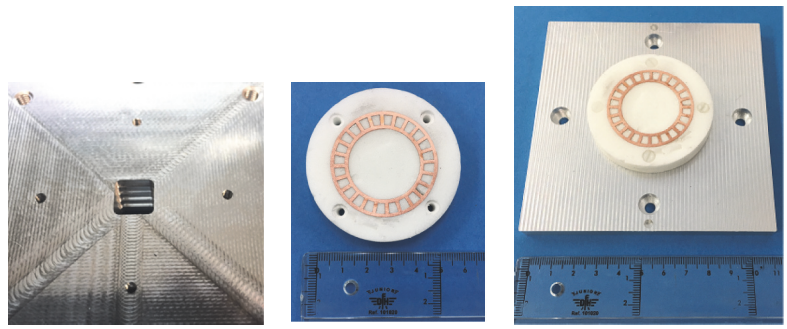

(a) (b) (c)

Figure 8: Photograph of the manufactured prototype of the proposed lens antenna: (a) feeder, (b) single-layer lens antenna, and (c) lens with feeder.

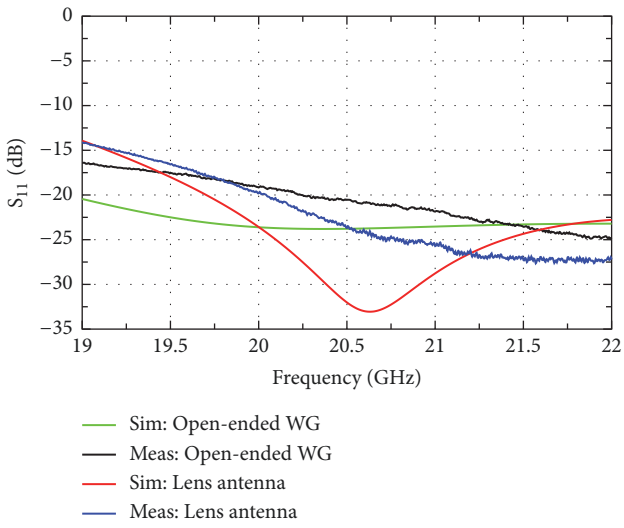

Figure 9: Simulated and measured S_{11} parameter of the proposed metallic lens antenna.

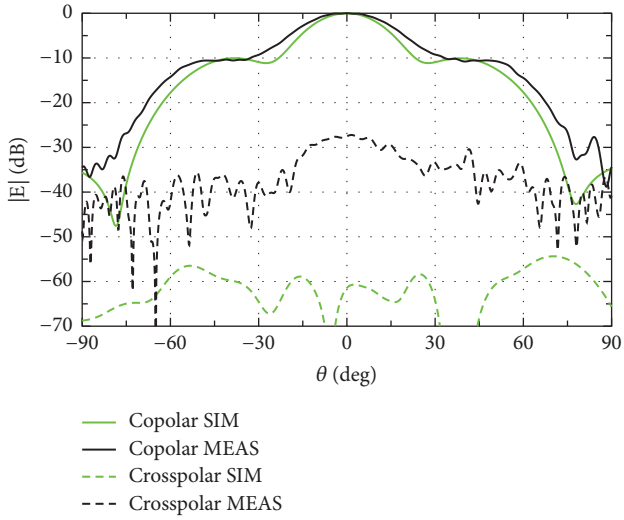

Figure 10: Measured (MEAS) and simulated (SIM) copolar and crosspolar components of the radiation pattern at 20.5 GHz.

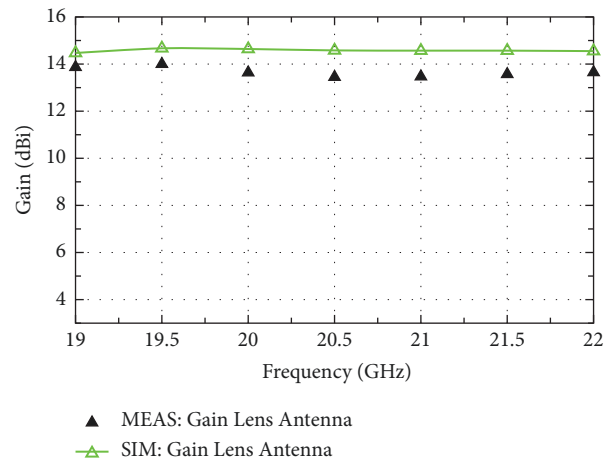

Figure 11: Comparison of the maximum gain, measured (MEAS) and simulated (SIM), of the proposed lens.

It can be clearly observed that the proposed antenna has an operational bandwidth of 14.7% for $|S_{11}| < -14$ dB, and a radiation efficiency above 90%.

5. Conclusion

A low profile metallic lens antenna formed by 2 short-circuited metallic rings has been proposed. The single-layer lens antenna has been designed using the Theory of Characteristic Modes to facilitate the design process and evaluate the performance of currents in the metallic structure. Note that a final optimization has not been required. An open-ended square waveguide is used as the primary feed for the metallic lens. The resulting structure improves the maximum directivity with respect to the feeder along a large bandwidth (more than 5 dB) and provides a good crosspolar level (better than -27 dB), with a measured directivity above 13.70 dB.

Data Availability

The simulation and measurement data used to support the findings of this study are available from the corresponding author upon request.

Conflicts of Interest

The authors declare that they have no conflicts of interest.

Acknowledgments

This work has been supported by the Spanish Ministry of Science, Innovation and Universities (Ministerio Ciencia, Innovación y Universidades) under the projects TEC2016-79700-C2-1-R and TEC2016-78028-C3-3-P and college scholarship graduate of the National University of Chimborazo.

References

[1] Y. Mao, C. You, J. Zhang, K. Huang, and K. B. Letaief, "A survey on mobile edge computing: the communication perspective," *IEEE Communications Surveys & Tutorials*, vol. 19, no. 4, pp. 2322–2358, 2017.

[2] D. Sanchez-Escuderos, H. C. Moy-Li, E. Antonino-Daviu, M. Cabedo-Fabres, and M. Ferrando-Bataller, "Microwave planar lens antenna designed with a three-layer frequency-selective surface," *IEEE Antennas and Wireless Propagation Letters*, vol. 16, pp. 904–907, 2017.

[3] O. Quevedo-Teruel, J. Miao, M. Mattsson, A. Algaba-Brazalez, M. Johansson, and L. Manholm, "Glide-symmetric fully metallic luneburg lens for 5G communications at Ka-band," *IEEE Antennas and Wireless Propagation Letters*, vol. 17, no. 9, pp. 1588–1592, 2018.

[4] E. G. Plaza, G. Leon, S. Loredo et al., "An ultra thin 2-bit near-field transmitarray lens," *IEEE Antennas and Wireless Propagation Letters*, vol. 16, pp. 1784–1787, 2017.

[5] S. H. Ramazannia Tuloti, P. Rezaei, and F. Tavakkol Hamedani, "High-efficient wideband transmitarray antenna," *IEEE Antennas and Wireless Propagation Letters*, vol. 17, no. 5, pp. 817–820, 2018.

[6] X. Y. Lei and Y. J. Cheng, "High-efficiency and high-polarization separation reflectarray element for OAM-folded antenna application," *IEEE Antennas and Wireless Propagation Letters*, vol. 16, pp. 1357–1360, 2017.

[7] M. Jiang, Z. N. Chen, Y. Zhang, W. Hong, and X. Xuan, "Metamaterial-Based Thin Planar Lens Antenna for Spatial Beamforming and Multibeam Massive MIMO," *IEEE Transactions on Antennas and Propagation*, vol. 65, no. 2, pp. 464–472, 2017.

[8] E. Kim, S. Ko, Y. J. Lee, and J. Oh, "Millimeter wave tiny lens antenna employing U-Shaped filter arrays for 5G," *IEEE Antennas and Wireless Propagation Letters*, vol. 17, no. 5, pp. 845–848, 2018.

[9] H. Li, G. Wang, J. Liang, X. Gao, H. Hou, and X. Jia, "Single-layer focusing gradient metasurface for ultrathin planar lens antenna application," *Institute of Electrical and Electronics Engineers. Transactions on Antennas and Propagation*, vol. 65, no. 3, pp. 1452–1457, 2017.

[10] M. Cabedo-Fabres, E. Antonino-Daviu, A. Valero-Nogueira, and M. F. Bataller, "The theory of characteristic modes revisited: a contribution to the design of antennas for modern applications," *IEEE Antennas and Propagation Magazine*, vol. 49, no. 5, pp. 52–68, 2007.

[11] R. Garbacz and R. Turpin, "A generalized expansion for radiated and scattered fields," *IEEE Transactions on Antennas and Propagation*, vol. 19, no. 3, pp. 348–358, 1971.

[12] R. F. Harrington and J. R. Mautz, "Theory of characteristic modes for conducting bodies," *IEEE Transactions on Antennas and Propagation*, vol. 19, no. 5, pp. 622–628, 1971.

[13] Z. Miers and B. K. Lau, "Wideband characteristic mode tracking utilizing far-field patterns," *IEEE Antennas and Wireless Propagation Letters*, vol. 14, pp. 1658–1661, 2015.

[14] E. Antonino-Daviu, M. Cabedo-Fabres, M. Sonkki, N. Mohamed Mohamed-Hicho, and M. Ferrando-Bataller, "Design guidelines for the excitation of characteristic modes in slotted planar structures," *IEEE Transactions on Antennas and Propagation*, vol. 64, no. 12, pp. 5020–5029, 2016.

[15] E. Antonino-Daviu, M. Cabedo-Fabrés, M. Ferrando-Bataller, and M. Gallo, "Design of a multimode MIMO antenna using the theory of characteristic modes," *Radioengineering*, vol. 18, no. 4, pp. 425–430, 2009.

[16] M. Capek, P. Hazdra, M. Masek, and V. Losenicky, "Analytical representation of characteristic mode decomposition," *IEEE Transactions on Antennas and Propagation*, vol. 65, no. 2, pp. 713–720, 2017.

[17] X. Yang, Y. Liu, and S. Gong, "Design of a wideband omnidirectional antenna with characteristic mode analysis," *IEEE Antennas and Wireless Propagation Letters*, vol. 17, no. 6, pp. 993–997, 2018.

[18] N. M. Mohamed-Hicho, E. Antonino-Daviu, M. Cabedo-Fabrés, and M. Ferrando-Bataller, "Designing slot antennas in finite platforms using characteristic modes," *IEEE Access*, vol. 6, no. 41, pp. 346–355, 2018.

[19] D. Santillán-Haro, E. Antonino-Daviu, D. Sánchez-Escuderos, and M. Ferrando-Bataller, "Analysis and design of a metamaterial lens antenna using the theory of characteristic modes," *International Journal of Antennas and Propagation*, vol. 2018, Article ID 6329531, 8 pages, 2018.

[20] D. Santillán-Haro, E. Antonino-Daviu, D. Sánchez-Escuderos, and M. Ferrando-Bataller, "Metamaterial lens design using characteristics modes," in *Proceedings of the Numerical Electromagnetic and Multiphysics Modeling and Optimization for RF, Microwave, and Terahertz Applications (NEMO)*, pp. 37–39, IEEE, 2017.

[21] D. Santillán-Haro, E. Antonino-Daviu, D. Sánchez-Escuderos, and M. Ferrando-Bataller, "Design of high-gain antennas for 5G systems using characteristic modes," in *Proceedings of the Antennas and Propagation Society International Symposium (APSURSI)*, pp. 1-2, IEEE, 2018.

[22] "Altair, Feko suite 7.0".

[23] *Dassault Systemes*, CST microwave studio, 2018.

[24] S. Karimkashi and A. A. Kishk, "Focusing properties of fresnel zone plate lens antennas in the near-field region," *IEEE Transactions on Antennas and Propagation*, vol. 59, no. 5, pp. 1481–1487, 2011.